Structural, Microstructural, and Residual Stress Investigations of Plasma-Sprayed Hydroxyapatite on Ti-6Al-4 V

Adele Carradó*

Institut de Physique et Chimie des Matériaux de Strasbourg, UMR 7504 UDS-CNRS, 23 rue du Loess, BP 43, 67034 Strasbourg Cedex 2, France

ABSTRACT Plasma-spray (PS) is a classical technique usually employed to cover orthopaedic titanium implant surfaces with hydroxyapatite (HA - $Ca_{10}(PO_4)_6(OH)_2$). The objective of the current study is to investigate the structure and microstructure of HA plasma-spray 50 μm thick coating on titanium alloy (Ti-6Al-4 V) and residual stress due to processing in the substrate and in HA coating. The structure of the coatings was determined by high-energy synchrotron X-ray diffraction in energy dispersive (HESXRD), selected area electron diffraction (saed), Scanning Electron Microscopy (SEM), and Fourier transform infrared spectroscopy (FTIR). No impurity phases in the HA were identified by HESXRD to keep away from the decomposition of HA at high temperature. hcp phase of HA substrate was detected with slight amorphous background. FTIR spectrum of a HA powder shows a typical spectrum for HA material with the characteristic phosphate peaks for HA at wavenumbers of 1090, 1052, 963, 602, and 573 cm^{-1} are present. The morphology of HA powder observed by SEM exhibits grains of ca. 0.1 μm well-adapted for cell proliferation. HA/Ti-6Al-4 V interface observed by cross-section scanning and transmission electron microscopy (TEM) presents microcracks. Residual stresses were analyzed by sin^2 Ψ X-ray diffraction method on titanium substrates and HA coating. Although the Ti substrates are in a slightly tensile residual state, the coated ones show a compressive state.

KEYWORDS: microstructure • nondestructive analysis • residual stress • coatings • plasma-spray deposition

1. INTRODUCTION

Calcium phosphate ceramics, especially hydroxyapatite, are currently used as biomaterials for many applications in dentistry and orthopaedics, because they form a real bond with the surrounding bone tissue when implanted (1). Hydroxyapatite (HA) ($Ca_{10}(PO_4)_6(OH)_2$), the major mineral component of bones and teeth, is one of the most-used materials for coating. Even so, because of the poor mechanical properties of bulk HA ceramics, they cannot be used as implant devices to replace large bony defects or for load-bearing applications as described by Hench (2). Wolke and K. De Groot (3) and Kay (4) reported that HA has low mechanical strength, but very good osteointegration and biocompatibility.

Titanium (Ti) and titanium alloys (Ti-6Al-4 V) are biocompatible materials and present good mechanical properties that can be used to realize fixed and mobile biomechanical prostheses, to be implanted inside the human body for a long time.

The use of HA coatings on titanium alloys leads to a structure that has good mechanical strength and good osteointegration properties at the surface and in the manufacturing of prosthetic devices. The system HA/Ti is used to improve the surface properties of the device and to induce osteointegration process (5, 6). Furthermore, it has been demonstrated that the bond between HA and bone is better than the bond between titanium and bone (7, 8).

A considerable amount of research has been devoted to develop techniques for coating calcium phosphate compounds on titanium for medical implantation such as plasma spraying (9, 10), dipping (11), electro-codeposition (12), pulsed-layer deposition (13), sputtering (13) and sol−gel-derived coating (14). The plasma-spray (PS) technique is a currently commercially available method for coating implant devices with HA. But the PS, although it exhibits a very good biocompatibility, also presents some disadvantages affecting the long-term stability of the implant and, therefore, its lifetime. Among these drawbacks, the most significant are the poor coating and substrate adherence and the lack of uniformity of the coating. To predict the location of failures, knowledge of the residual internal stress induced in thermally sprayed coating during deposition is important. The natural stress relaxation mechanism, through a network of microcrack development in the ceramic coating volume, is another important factor to be considered for interface failure analysis. During the clinical use of hydroxyapatite coated implants, the mechanical stresses are added to the pre-existing residual stresses. The magnitude of these cumulated stresses affects the coating's performances (15–18).

In this paper, structural and morphological results are reported as well as residual strain studies using a nondestructive method such as X-ray diffraction measurements performed on coated Ti substrates as well as on HA coatings. The morphology in correlation with residual stress evaluation is an important to improve of the biomaterials perfor-

Table 1. Characteristic Data of Titanium Alloy and Hydroxyapatite: Crystalline Structure, Lattice Parameters, Elastic Modulus (E), Poisson's ratio (ν), Radio-Crystallographic Constants (S_1 and S_2) and Coefficient of Thermal Expansion (α)

	structure	$a = b$ (nm)	c (nm)	E (GPa)	ν	$S_1 = \nu/E_{hkl}$ (M Pa^{-1})	$1/2S_2 = (1 + \nu)/E_{hkl}$ (M Pa^{-1})	α (ppm/K^{-1})
Ti-6Al-4 V	hcp	0.29505	0.46826	110	0.34	−3.09	12.18	8.5
HA	hpc	0.94075	0.68775	108	0.28	−2.39	10.94	14

mances, the control of deformations, the components' lifetime and given a better understanding of industrial processing.

2. EXPERIMENTAL PROCEDURE

2.1. HA Coating. 50 μm HA coatings were deposited by plasma-spray on square pieces ($10 \times 10 \times 1$ mm^3) of Ti-6Al-4 V (elem %: C, 0.013; Fe, 0.16; N, 0.014; H$_2$, 0.006; O, 0.11; Al, 6.05; V, 4.0; Ti, bal.). Prior to the coating procedure, a degreasing and grit-blasting surface treatment with alumina powder (14 μm) was performed in order to guarantee a minimum adhesion of the coating introducing a grit-blasting surface treatment. Some characteristic of Ti-6Al-4 V and HA are given in Table 1.

2.2. Phase, Structure, and Morphology Characterization. Commercial HA powder (©Flametal) and Ti-6Al-4 V substrate were subjected to High-Energy Synchrotron X-ray Diffraction (HESXRD) performed at ID15A ESRF beam line (Grenoble, France) by white-beam energy ranged from 20 to 150 keV at a fixed scattering angle $2\theta = 5°$ to precisely study their phases.

A 3-axes diffractometer equipped with an Eulerian cradle was used. The gauge volume was limited to $60 \times 700 \times 100$ μm^3 by slits in the incident and in the diffracted beam.

In addition, Fourier transform infrared (FTIR) spectra were obtained by FTIR spectroscopy in the range 200−4000 cm^{-1} with a 4 cm^{-1} resolution.

For structural investigation of HA coating, selected area electron diffraction (SAED) was performed with a Topcon EM 002B electron microscope operating at 200 kV with a 0.18 nm point to point resolution, equipped with a low dose camera and a Si/Li detector for analysis. To prepare a cross section transmission electron microscopy (XTEM), a slice was cut perpendicular to the surface of sample by focused ion beam (FIB) milling and sputtered with a Pt layer before thinning the sample. Previous work s (19, 20) demonstrated that the FIB technique can be successfully applied to XTEM sample preparations without noticeable ion beam-induced damages.

Morphological characterisation of HA powder and HA/Ti-6Al-4 V interface were observed by scanning electron microscopy (SEM) using JEOL JSM-6700F field emission microscope.

2.3. Residual Stress Analysis by X-ray Diffraction. The general principles of X-ray evaluations are based on the measurement of lattice parameters in different directions of the specimen (Figure 1). The value of strain of a material is obtained by measuring the shift of angle peak. The stress components are then calculated from the lattice strains using stress/strain

relations obtained through a mechanical approach of the polycrystalline aggregate. In the case of anisotropic homogeneous elastic continuous medium, a simple equation can generally be used being called sin^2 Ψ law. The stress σ_ϕ is determined by

$$\sigma_\phi = \frac{E}{(1 + \nu)\sin \psi}\frac{d - d_0}{d_0}$$

where E is the Young's modulus, ν Poisson's ratio, and d_0 and d initial and measured inter-planar distances. ϕ is the angle between a fixed direction in the plane of the sample and the projection in that plane on the normal diffracting plane, and Ψ is the angle between the normal of the sample and the normal of the diffracting plane. The stress distribution is then described by the stress components σ_{11}, σ_{12}, and σ_{22} in the plane of the surface, with no stress acting perpendicular to the free surface (σ_{33}) (Figure 1). The normal component σ_{33} and the shear stresses $\sigma_{13} = \sigma_{31}$ and $\sigma_{23} = \sigma_{32}$ acting out of the plane of the sample surface are zero. Stress determination was supposed to be done in a monophased material.

The sprayed HA coatings on the Ti-6Al-4 V substrate were examined by X-ray diffraction using a computer-controlled Philips diffractometer. Diffraction scans were run with a generator voltage of 40 kV and a generator current of 40 mA. Receiving slit of 0.1 mm width was used. For both HA coatings and Ti-6Al-4 V substrates, each diffraction scan was done at ψ angles (±45, ±40.2, ±35.26, ±30, ±24.09, and ±16.78°), and ϕ angles (0, 45, and 90°) with a step (2θ) of 0.02° (scan time of 60 s) for the HA coating and 0.05° (scan time of 8 s) for the Ti-6Al-4 V substrate. Cu−K$_{\alpha1}$ and Cu−K$_{\alpha2}$ radiation ($\lambda_1 =$ 0.154056 nm and $\lambda_2 =$ 0.154439 nm) were used.

3. RESULTS AND DISCUSSION

Commercial HA powder with particles size in the range of 10−80 μm (Figure 2a) was used for the production of composite powder. HA powder surface analysis by SEM illustrated the coarsening (Figure 2b) and subsequent sintering (Figure 2c) of the micrometer crystallites that constitute a powder particle. No impurity phases, i.e., tetracalcium phosphate (TTCP), α-tricalcium phosphate (TCP), etc., could be identified by HESXRD (Figure 3a), and hindering the decomposition of HA at high temperature. Crystalline phase of HA substrate (hcp crystal symmetry) was detected and the evolution of the background noise shows a negligible amorphous background. α- (hcp) and β- (bcc) Ti phases were observed in the Ti6Al4 V alloy with β-Ti in a smaller volume fraction (Figure 3b) and being not considered in the residual strain evaluation.

The stretching bands at 3571 cm^{-1}, libration bands at 635 cm^{-1} originating from OH$^-$ groups, as well as characteristic bands due to PO$_4^{3-}$ ions are clearly visible in Figure 4 (21–23). The latter ones are as follows: the ν_1 band at about 963 cm^{-1}, the ν_3 band at 1090 and 1052 cm^{-1}, and the ν_4 bands at 573 and 602 cm^{-1} (21–23, 24).
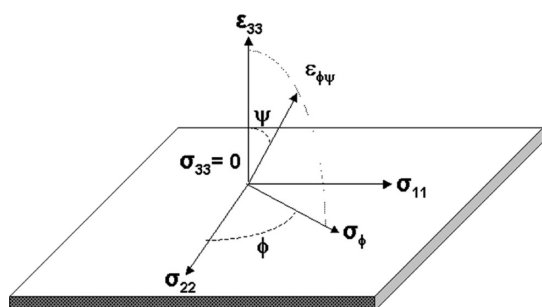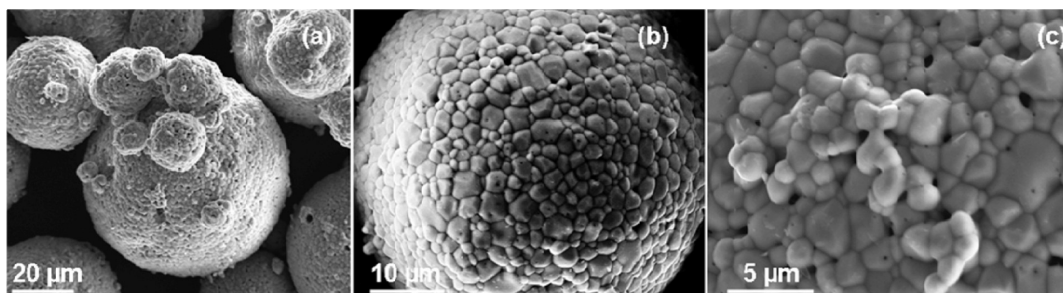

FIGURE 1. Plane-stress conditions.

FIGURE 2. SEM micrographs at different magnifications of HA commercial powder: (a) size of particles is between 10 and 80 μm; (b) particle surface is uneven and jagged; (c) crystallized size is in the range of 0.1−3 μm.
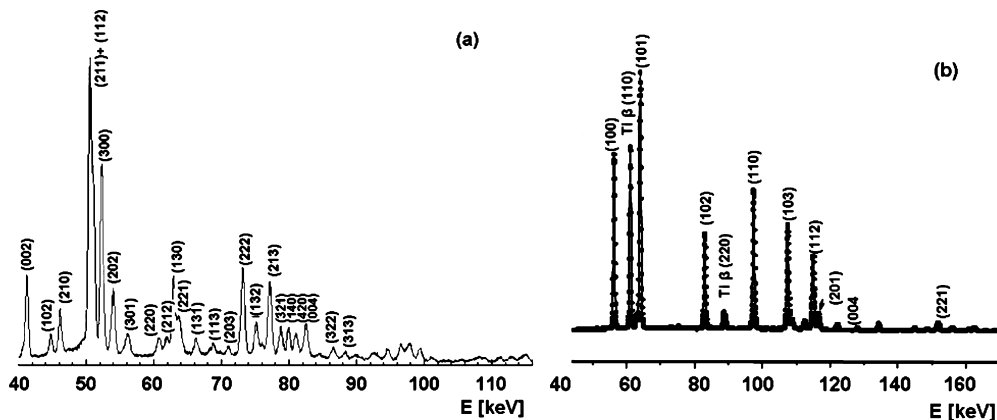

FIGURE 3. HESXRD pattern plotted as a function of energy using incidence angle $2\theta = 5°$: (a) hcp crystalline phase HA powder and (b) α- (hcp) and β- (bcc) Ti phases in Ti-6Al-4 V substrate.
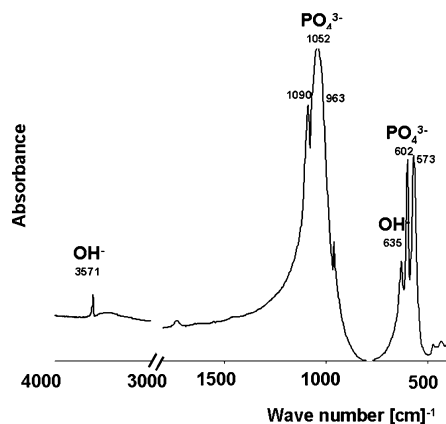

FIGURE 4. Fourier transform infrared spectra of HA powder.

SAED pattern (Figure 5a) was performed to prove the crystalline structure characteristic to HA (Figure 5b). Diffraction spots, characteristic to the (101) crystallographic planes of HA, were identified in agreement with the occurrence of small domains with crystalline grains. During the HA deposition, the layer is made up by single-crystal stacking of grains (1.5×1.4 μm^2, Figure 5b), which are a succession of the droplets of molten material coated by plasma spray.

In Figure 6, a cross-section SEM micrograph of the interface between the porous HA coating and Ti-6Al-4 V substrate is shown. The microscopic examination of the HA/Ti-6Al-4 V cross-section may provide an overview of the possible repercussion of the morphology in the mechanical properties of the coatings and offer information directly related to their bond strength performance (25). As shown in Figure 6, SEM cross-section reveals the presence of a crack

in the Ti-6Al-4 V substrate (a) and along the coating-substrate interface (b). Moreover, the HA layer presents an important porosity after grit-blasting between the various grains, associated with the high fabrication temperature. The surface roughness of the substrate is particularly important in HA coating not only because a rough surface can provide increased wettability of the HA solution on the substrate but also because mechanical interlocking between the HA-coated layer and substrate may be enhanced (26). The poor bond strength revealed by the plasma-spray coatings and the need of a grit-blasting step before the coating process, proof that these coatings are not in truth adherent to the substrate, as it is only mechanically anchored to the inhomogeneities introduced in the titanium by the grit blasting as show in X-TEM (Figure 7).

In Figure 8, it can be observed the residual stress state for the HA coating, on the bare Ti-6Al-4 V substrate as well as on HA layer at $\phi = 0$, 45, and 90° with respective values of stress. In the Ti-6Al-4 V substrate, residual stresses at $\phi = 0$, 45° were negligible (13 ± 6 MPa; 6 ± 3 MPa), whereas at $\phi = 90°$ they were found slightly tensile (66±7 MPa). On the contrary the residual stresses in HA at 0, 45, and 90°, with respect to the spraying direction for the HA coatings were all in compressive state (−109 ± 15 MPa; −78 ± 24 MPa, and −127 ± 13 MPa). There was no obvious difference in direction between the major principal residual stress (σ_{11}) and the RS in spraying direction ($\phi = 0°$) in the surface of HA.

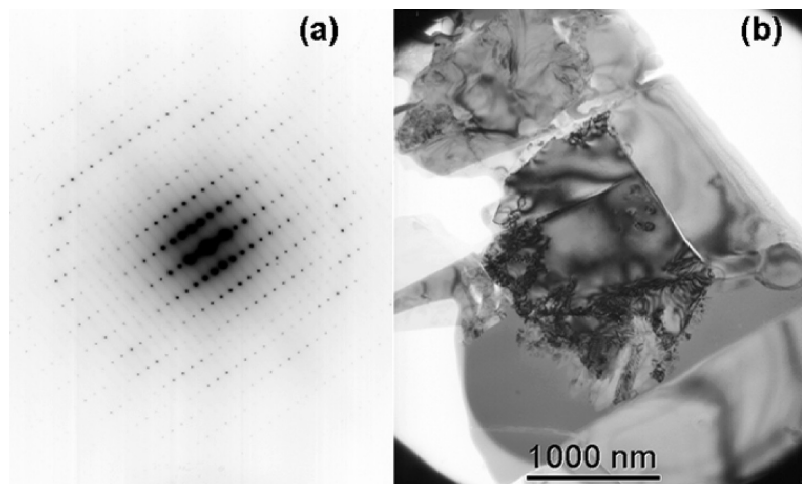Residual stresses of plasma-spray coating arise from the intrinsic or deposition stresses, which are generated during

FIGURE 5. (a) SAED pattern of HA crystalline structure and (b) 1.5×1.4 μm^2 HA grain size in Bragg contrast.
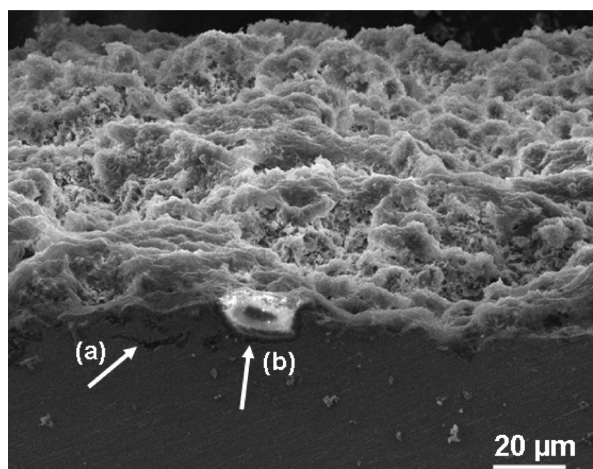

FIGURE 6. SEM micrograph of the HA/ Ti-6Al-4 V interface. Plasma-spray HA layer showing the typical splat-shaped structure, with interconnecting porosity. Cracks are present in (a) the Ti-6Al-4 V substrate and (b) along the coating−substrate interface.

the cooling of sprayed particles to substrate temperature after solidification or because of differential thermal contraction arising during post-fabrication cooling down (27). The behavior and mechanism of residual stress generation are so complicated that a small numbers of previous works were able to quantitatively predict the magnitude of residual stress.

The thermal expansion coefficient of sintered HA was larger than that of Ti-6Al-4 V alloy ($\alpha_{HA} = 14 \times 10^{-6}$ K^{-1}, $\alpha_{Ti-6Al-4\ V} = 8.5 \times 10^{-6}$ K^{-1}, respectively) (Table 1), hence the HA might result in a tensile stress state after being cooled from the elevated temperature. However, this is still an open point. As Yanga and Chang (28) reported, the thermal expansion coefficient of the plasma-sprayed HA is not known. The temperatures of HA and substrate are not equal and homogeneous with each other and in the respective material. Therefore, it is incorrect to calculate the residual stress of HA even though the thermal expansion coefficients of HA and Ti-alloy were experimentally available. Moreover, the value of the HA Young's modulus depends on the characteristic and structure of materials, being different in the same material arising from different processes or meth-
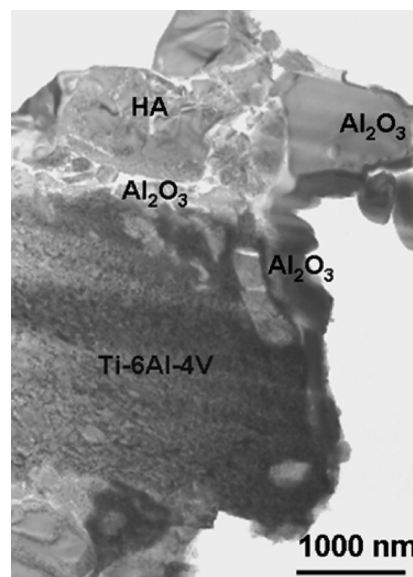

FIGURE 7. FIB slice observed by X-TEM. HA and titanium alloy are mechanically anchored and the presence of alumina introduced in the titanium by grit blasting.
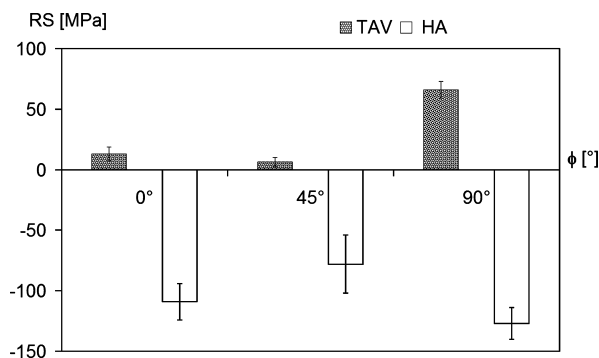

FIGURE 8. Residual stress state on the bare Ti substrates as well as on HA layers.

ods. Sergo et al. (29) reported that the Young's modulus of HA might be a function of porosity but no data were provided. In other literature, however, a correlation of the Young's modulus and the volume fraction of porosity were established (30). Theoretical Young's modulus of a dense and sintered bulk HA was reported as being approximately

110 GPa (31–33), though a lower value of 34.5 GPa was noted, too (34).

Although it has become evident that residual stress had the greatest detrimental effect on the bonding at the interface of the HA coating and the Ti-substrate, it had less of an adverse effect on the cohesive bonding in the lamellar splats or at lamellar-splat boundaries.

CONCLUSIONS

Although plasma spray technique is currently employed to produce coatings used clinically, the long-term stability of the coating/implant is questionable. PS coating implant devices with HA showed disadvantages, affecting the long-term stability and lifetime of implant. In spite of microstructural and structural successful results, these investigations of plasma-sprayed ceramic coatings on metal substrates have shown failure at interface. Moreover, as suggested from mechanical measurements, compressive residual stresses occurring in the coating and the substrate are a positive point for the lifetime of system.

A considerable amount of new research has been dedicated to improving and developing deposition techniques for calcium phosphate coating compounds on titanium for medical application such as pulsed-layer deposition, sputtering, and sol−gel-derived coating.

REFERENCES AND NOTES

(1) Legeros, R. Z. *Adv. Dent. Res.* **1988**, *2*, 164.
(2) Hench L. L., Wilson J. Introduction. In *An Introduction to Bioceramics*; Hench, L. L., Wilson, J., Eds.; Advanced Series in Ceramics; World Scientific: Singapore, 1993; Vol. 1, pp 1−24.
(3) Koch, B.; Wolke, J. G. C.; De Groot, K. *J. Biomed. Mater. Res.* **1990**, *24*, 655.
(4) Kay, J. F. *Dent. Clin. North Am.* **1992**, 36.
(5) Lacefield, W. R. *Implant Dent.* **1998**, *7*, 315–22, 4.
(6) Rokkum, M.; Reigstad, A. *J. Arthroplasty* **1999**, *14, 6*, 689–700, 1−2.
(7) Radin, S. R.; Ducheine, P. *J. Mater. Sci. Mater. Med.* **1992**, *3*, 33.
(8) Filiaggi, M. J.; Pilliar, R. M.; Coombs, N.A. *J. Biomed. Mater. Res.* **1993**, *27*, 91.
(9) Yang, C. Y.; Wang, B. C.; Chang, E.; Wu, J. D. *J. Mater. Sci. Mater. Med.* **1995**, *6*, 249.
(10) Weng, J.; Liu, X. G.; Li, X. D.; Zhang, X. *J. Mater. Sci. Mater. Med.* **1996**, *7*, 355.
(11) Li, T. T.; Lee, J. H.; Kobaysi, T.; Aoki, H. J. *Mater. Sci.: Mater. Med.* **1996**, *7*, 355.
(12) Dasarathy, H.; Riley, C.; Coble, H. D.; Lacefield, W. R.; Maybee, G. *J. Biomed. Mater. Res.* **1996**, *31*, 81.
(13) Cotell, C. M. In *Pulsed laser deposition of biocompatible thin films*; Chrisey, D. B., Hubler, G. K., Eds.; Pulsed Laser Deposition of Thin Films; Wiley: New York, 1994; p 549.
(14) Weng, W.; Baptista, J.L. *J. Mater. Sci. Mater. Med.* **1998**, *9*, 159.
(15) Yang, C. Y.; Wang, B. C.; Lee, T. M.; Chang, E.; Chang, G.L. *J. Biomed. Mater. Res.* **1997**, *36*, 39–48.
(16) Hayashi, K.; Inadome, T.; Tsumura, H.; Nakashima, Y.; Sugioka, Y. *Biomaterials* **1994**, *15* (14), 1187–1191.
(17) Wang, S.; Lacefield, W. R.; Lemons, J. E. *Biomaterials* **1996**, *17* (20), 1965–1970.
(18) Elsing, R; Knotek, O; Balting, U. *Surf. Coat. Technol.* **1990**, *43−44*, 426–435.
(19) Heaney, P. J.; Vicenzi, E. P.; Giannuzzi, L. A.; Livi, K. J. T. *Am. Mineral.* **2001**, *86*, 1094.
(20) Lipp, S.; Frey, L.; Lehrer, C.; Frank, B.; Demm, E.; Rysell, H. *J. Vac. Sci. Technol., B* **1996**, *14*, 3996.
(21) Slŏsarczyk, A.; Paluszkiewicz, C.; Gawlicki, M.; Paszkiewicz, Z. *Ceram. Int.* **1997**, *23*, 297–304.
(22) Rapacz-Kmita, A.; Slŏsarczyk, A.; Paszkiewicz, Z.; Paluszkiewicz, C. *J. Mol. Struct.* **2004**, *704*, 333–340.
(23) Fowler, B. O. *Inorg. Chem.* **1974**, *1*, 194–207.
(24) Park, E.; Condrate, R. A.; Lee, D. *Mater. Lett.* **1998**, *36*, 38–43.
(25) Garcia-Sanz, F. J.; Mayor, M. B.; Arias, J. L.; Pou, J.; Leo, B.; Perez-Amor, M. *J. Mater. Sci. Mater. Med.* **1997**, *8*, 861–865.
(26) Changkook, Y.; Sunho, O.; Sukyoung, K. *J. Sol−Gel Sci. Technol.* **2001**, *21*, 49–54.
(27) Yang, Y.C.; Chang, E *Biomaterials* **2001**, *22*, 1827–1836, 13.
(28) Yanga, Y.C.; Chang, E. *Surf. Coat. Technol.* **2005**, *190*, 122–131.
(29) Sergo, V.; Sbaizero, O.; Clarke, D. R. *Biomaterials* **1997**, *18*, 477–482.
(30) Coble, R. L.; Kingery, W. D. *J. Am. Ceram. Soc.* **1956**, *39*, 11–381.
(31) Ravaglioli A., Krajewski A. *Bioceramics: Materials, Properties, Application*; Chapman & Hall: London, 1992.
(32) de With, G.; Vandijk, H.J.A.; Hattu, N.; Prijs, K. *J. Mater. Sci.* **1981**, *16*, 1592–1598.
(33) Kats J. L., Harper R. A. Calcium phosphate and apatites. In *Concise Encyclopaedia of Medical and Dental Materials*; Williams, D., Ed.; Pergamon Press: New York, 1990; pp 87−95.
(34) Jacho, M.; Bolen, C. H.; Thomas, M. B.; Bobick, J.; Kay, J. F.; Doremus, R. H. *J. Mater. Sci.* **1976**, *11*, 2027–2035.

AM900763J